JGP Journal of General Physiology

ARTICLE

# Relaxed tarantula skeletal muscle has two ATP energy-saving mechanisms

Weikang Ma[1], Sebastian Duno-Miranda[2], Thomas Irving[1], Roger Craig[3], and Raúl Padrón[3]

**Myosin molecules in the relaxed thick filaments of striated muscle have a helical arrangement in which the heads of each molecule interact with each other, forming the interacting-heads motif (IHM). In relaxed mammalian skeletal muscle, this helical ordering occurs only at temperatures >20°C and is disrupted when temperature is decreased. Recent x-ray diffraction studies of live tarantula skeletal muscle have suggested that the two myosin heads of the IHM (blocked heads [BHs] and free heads [FHs]) have very different roles and dynamics during contraction. Here, we explore temperature-induced changes in the BHs and FHs in relaxed tarantula skeletal muscle. We find a change with decreasing temperature that is similar to that in mammals, while increasing temperature induces a different behavior in the heads. At 22.5°C, the BHs and FHs containing ADP.$P_i$ are fully helically organized, but they become progressively disordered as temperature is lowered or raised. Our interpretation suggests that at low temperature, while the BHs remain ordered the FHs become disordered due to transition of the heads to a straight conformation containing Mg.ATP. Above 27.5°C, the nucleotide remains as ADP.$P_i$, but while BHs remain ordered, half of the FHs become progressively disordered, released semipermanently at a midway distance to the thin filaments while the remaining FHs are docked as swaying heads. We propose a thermosensing mechanism for tarantula skeletal muscle to explain these changes. Our results suggest that tarantula skeletal muscle thick filaments, in addition to having a superrelaxation–based ATP energy-saving mechanism in the range of 8.5–40°C, also exhibit energy saving at lower temperatures (<22.5°C), similar to the proposed refractory state in mammals.**

## Introduction

The smallest unit of striated muscle is the sarcomere, formed primarily by the interdigitation of myosin-containing thick filaments and actin-containing thin filaments. Muscle contraction occurs by the active sliding of the thin filaments along the thick filaments, powered through the cross-bridge cycle, and initiated by an increase of [$Ca^{2+}$] that switches on the thin filaments via the troponin complex and tropomyosin. Relaxation occurs when this sliding is stopped by a [$Ca^{2+}$] decrease. Understanding the structure of both sets of filaments, including the roles of the myosin heads, that, when bound to the thin filament, constitute the cross-bridges is key to understanding the molecular mechanism of muscle contraction and its regulation by [$Ca^{2+}$].

The thick filament is formed by self-assembly of myosin II molecules, whose tails pack together in the filament backbone and whose heads lie on its surface. The structure of thick filaments has been elucidated by low-angle x-ray diffraction (XRD) and EM. XRD has shown that the myosin heads are helically, or quasihelically, arranged in intact invertebrate and vertebrate muscles in the relaxed state (Huxley and Brown, 1967; Wray et al., 1975), while cryo-EM of tarantula skeletal muscle thick filaments shows that the two heads of each molecule in these helices have a bent conformation (in which the light chain domain is at an angle to the motor domain) such that one head ("blocked" head [BH]) and the other head ("free" head [FH]) interact with each other, as found in frozen-hydrated 2-D crystals (Wendt et al., 2001), and interact with myosin subfragment 2 (S2), forming the J motif, also known as the interacting-heads motif (IHM; Fig. 1 A; Alamo et al., 2008, Alamo et al., 2016, Alamo et al., 2017). The BH–FH interaction inhibits the activity of the two heads, contributing to the relaxed state of the thick filament. The IHM has been found to be present in all animals studied so far, by EM of isolated myosin II molecules and isolated thick filaments of vertebrate

[1]Biophysics Collaborative Access Team, Department of Biological Sciences, Illinois Institute of Technology, Chicago, IL; [2]Department of Molecular Physiology and Biophysics, Cardiovascular Research Institute, University of Vermont, Burlington, VT; [3]Division of Cell Biology and Imaging, Department of Radiology, University of Massachusetts Medical School, Worcester, MA.

Correspondence to Raúl Padrón: raul.padron@umassmed.edu

This work is part of a special collection on myofilament function and disease.

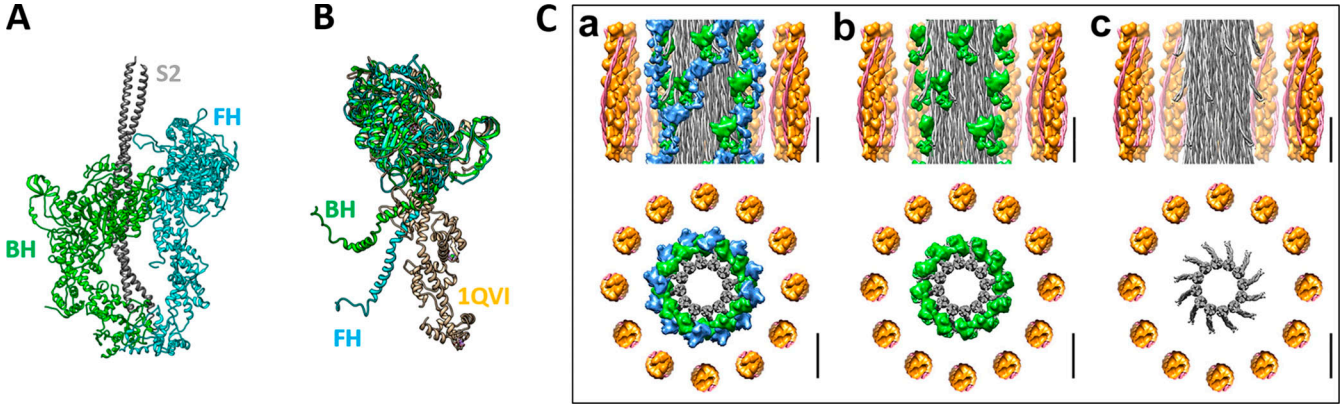


Figure 1. **The tarantula skeletal muscle myosin IHM.** Related to PDB accession no. 3JBH. **(A)** IHM with the BH and the FH shown in green and blue, respectively, and S2 shown in gray. **(B)** Superimposed motor domains of the IHM PDB 3JBH FH and BH as compared with the crystal structure of scallop myosin PDB accession no. 1QVI (in tan) representing the "prepower stroke" bent conformation (2.6 Å resolution; *Argopecten irradians*; Gourinath et al., 2003) with the BH and FH lever arms angled to allow the formation of the IHM (see Fig. 7). **(C)** Tarantula skeletal muscle lattice model showing a segment of relaxed tarantula skeletal muscle thick filament formed by two sets of BH (green) and FH (blue) helices above the myosin tails (gray), surrounded by 12 thin filaments (a). In the upper images, only the lateral thin filaments are shown. In b, the helices of FHs are removed, and in c, both sets of BHs and FHs are removed, leaving only the S2s and tails. Scale bars, 14.5 nm.

and invertebrate muscle (Lee et al., 2018; Alamo et al., 2018), and is therefore thought to be a fundamental property of the relaxed state.

XRD has shown that, in mammals, the organization of the heads in skinned, relaxed skeletal muscle is temperature dependent: helical ordering is present above 20°C, but this ordering declines at lower temperatures (Wray, J.S. 1987. Structure of relaxed myosin filaments in relation to nucleotide state in vertebrate skeletal muscle. J. Muscle Res. Cell Motil. 8: 62). This appeared to be an intrinsic property of the relaxed filaments, as it was independent of ionic conditions and filament overlap (Wray, J.S. 1987. Structure of relaxed myosin filaments in relation to nucleotide state in vertebrate skeletal muscle. J. Muscle Res. Cell Motil. 8:62). Disordering at lower temperatures appeared to be due to displacement of the Mg.ATP ⇔ Mg.ADP.$P_i$ equilibrium of the myosin-bound nucleotide in favor of the unhydrolyzed state. These findings were supported by further x-ray studies showing that, in skinned relaxed rabbit psoas muscle, the myosin layer lines (MLLs) in the x-ray pattern, which arise from the helical organization, were very weak at 0°C and increased steadily in intensity up to 20°C (Xu et al., 2003). These x-ray findings were supported by EM of relaxed thick filaments from rabbit, which showed disordering below 19°C compared with 25°C (Kensler et al., 1994), and from chicken pectoralis muscle, which revealed disorder near 4°C and order at 25°C (Kensler and Woodhead, 1995). Recently, it has been proposed that low temperature traps myosin heads in live mouse muscle in a refractory state that prevents activation (Caremani et al., 2019). Whether this refractory state occurs in other muscle systems is currently unknown.

This thermosensing effect in relaxed mammalian muscle was interpreted as being due to a redistribution of the heads between three distinct populations: (1) heads ordered on the thick filament backbone, (2) heads disordered but unattached to actin, and (3) heads weakly attached to actin (Malinchik et al., 1997). X-ray studies using analogues of ATP and ADP.$P_i$ showed that the change in ordering was due not to the nucleotide state itself (as originally thought) but to the effect of temperature on head conformation (helical order requires a bent conformation, which can form the IHM, while the straight conformation cannot form it). Mg.ADP.$P_i$ induces ordering by favoring the bent conformation, while ATP favors the straight conformation and thus disordering (Xu et al., 2003). EM studies in relaxed tarantula skeletal muscle thick filaments using analogues supported the view that Mg.ADP.$P_i$, which induces the bent conformation of the myosin head, favored helical ordering, while ATP induced disordering (Zoghbi et al., 2004).

In a recent x-ray study, we demonstrated that helically ordered IHMs characterize the relaxed state of live tarantula muscle, and we found evidence for different roles and dynamics for the BHs and FHs in these muscles during contraction (Padrón et al., 2020). Here, we take advantage of our understanding of the helical head organization in tarantula skeletal muscle to determine the effects of temperature on the BH and FH to better understand their possible different roles in the cross-bridge cycle and ATP energy saving. We found that the transition to disorder when lowering the temperature is similar to that in mammals. Surprisingly, we also observed disordering of the myosin helices when temperature was increased, a phenomenon not observed in previous studies with mammals. We propose a thermosensing mechanism, in the context of the cross-bridge cycle for tarantula skeletal muscle, that can explain the observed behavior of the BH and FH heads and suggests the existence of two ATP energy-saving mechanisms.

## Materials and methods

### Muscle preparations

#### *Leg segments*

Texas brown *Aphonopelma hentzi* tarantulas (Carolina Biological Supply Co.) were anesthetized with $CO_2$ (Lewbart, 2012). Their legs were excised quickly above the trochanter and immersed in tarantula Ringer solution (190 mM NaCl, 2 mM KCl, 4 mM $MgCl_2$,

1 mM $Na_2HPO_4$, and 4 mM $CaCl_2$, pH 7.5; Schartau and Leidescher, 1983) before mounting, with the exoskeleton intact, in the x-ray chamber.

### *Single isolated muscles*

The tarantula femur contains several muscles, whose nomenclature is not well defined (Dillon, 1952; Ruhland, 1978). The femur was immersed in Ringer solution, and only the muscle with a clearly defined tendon attached to the edge of the patella at the end distal to the trochanter and a robust muscle–cuticle attachment to the trochanter at the proximal end was dissected. We termed this the "flexor femoris cbensis", consisting of two muscle bundles (big and small) fused at the distal end (see Video 1 for dissection details). The small bundle was carefully stripped from the muscle before positioning the large bundle in the x-ray chamber.

### *Use of leg and isolated muscles*

Tarantula leg segments are covered by a hermetic exoskeleton, joined by sealed joints, containing hemolymph. Spiders move forward by a coordinated leg mechanism, driven first by contraction of muscles in the cephalothorax, which forces hemolymph into the legs, causing their extension, followed by flexing of the extended leg, which pulls the animal forward. We studied here the effect of temperature on the leg muscles of this tarantula species, that, together with the cephalothorax muscles (not studied here), contribute to its locomotion. In the intact, live leg (ex vivo), the muscles are in situ, surrounded by hemolymph. We compared the results from this preparation with those from one specific isolated muscle surrounded by tarantula Ringer solution. The XRD patterns were very similar (Fig. 2 A), suggesting that the muscle response per se was the important factor regarding the effect of temperature. The range of the temperature of the solution bathing the legs or isolated muscles was 8.5–40°C, but, for technical reasons, it was not possible to set the chamber temperature outside this range. We found that at 22.5°C the helical ordering is maximal (Fig. 3 A), exhibiting an optimal temperature ($t_{op}$) range of 20–27.5°C (see Fig. 6 A) approximately centered on the annual fluctuation range for this species.

### XRD

XRD experiments were performed using the small-angle XRD instrument at the Biophysics Collaborative Access Team (BioCAT) beamline 18ID at the Advanced Photon Source, Argonne National Laboratory (Fischetti et al., 2004). The x-ray beam energy was set to 12 keV (0.1033-nm wavelength) with an incident flux of ∼$10^{13}$ photons per second in the full beam. The x-ray beam was focused to ∼250 µm × 250 µm at the sample position and to ∼150 µm × 30 µm (horizontal × vertical) at the detector. The specimen-to-detector distance was ∼3 m. 20 images were collected at 10-ms exposure time with 10 ms between each frame using a Pilatus 3 1M detector (Dectris Inc.).

### *Leg segments*

An isolated whole leg was placed inside a customized chamber, with the femur horizontal and in the x-ray beam. For these intact segments, all femur muscles are present, producing a superposition of x-ray patterns with different orientations. We therefore first scanned the femur, taking single patterns at different locations, to find regions where most of the fibers had the same orientation, and then examined these regions in our experiments.

### *Isolated muscles*

For single isolated muscle experiments ($n$ = 3), the muscle was isolated with one free end and the other end still attached to part of the exoskeleton. The free end of the muscle fiber was attached to a force transducer via a T clip while the other end was attached to a static hook via the exoskeleton.

### Temperature experiments

The bottom of the chamber was attached to an aluminum heat exchanger for temperature control. A thermocouple was inserted into the solution for ambient temperature monitoring. The first pattern was taken between 22°C and 23°C. For ex vivo (whole-femur) experiments ($n$ = 3), the legs were either cooled down or heated up using the heat exchanger, and at least two patterns were taken every ∼4°C down to 8°C or up to 40°C (different legs were used for the heating and cooling experiments; $n$ = 3 each). The temperature measurement error was ±1°C. The x-ray data from the two groups of experiments, cooling or heating, were normalized against their values at 22–23°C to construct a complete curve. For isolated muscle experiments ($n$ = 3), the muscle was first cooled down with at least two patterns taken every ∼4°C down to 12°C. Then the muscle was allowed to return to its initial temperature (22–23°C) for at least 5 min, and a pattern was taken (similar in appearance to the starting pattern). The muscle was then heated to 34°C, with two patterns taken every ∼4°C and a final pattern taken again at the starting temperature of 22.5°C to test for reversibility. The results from two or more patterns at each temperature were averaged for statistical analysis.

### X-ray data analysis

The 20 10-ms exposures taken at each temperature point were summed together using Fit2d (Hammersley, 2016) for further analysis. The data were analyzed as described previously (Ma et al., 2018a; Ma et al., 2018b) using data analysis programs belonging to the MuscleX (version 1.13) software package developed at BioCAT (Jiratrakanvong et al., 2018). Briefly, in MuscleX, the images were quadrant folded and background subtracted using the "Quadrant Folding" routine; the spacing and intensities from equatorial reflections were measured using the "Equator" routine; and the spacing and intensities of the meridional reflections and layer lines were measured using the "Projection Traces" routine.

### Statistics

Statistical analyses were performed using GraphPad Prism 7 (GraphPad Software). The results are given as mean ± SEM unless otherwise stated. Symbols on figures: ns, $P \geq 0.05$; *, $P < 0.05$; **, $P < 0.01$; ***, $P < 0.001$; and ****, $P < 0.0001$ for two-tailed unpaired Student's $t$ tests, unless otherwise stated.

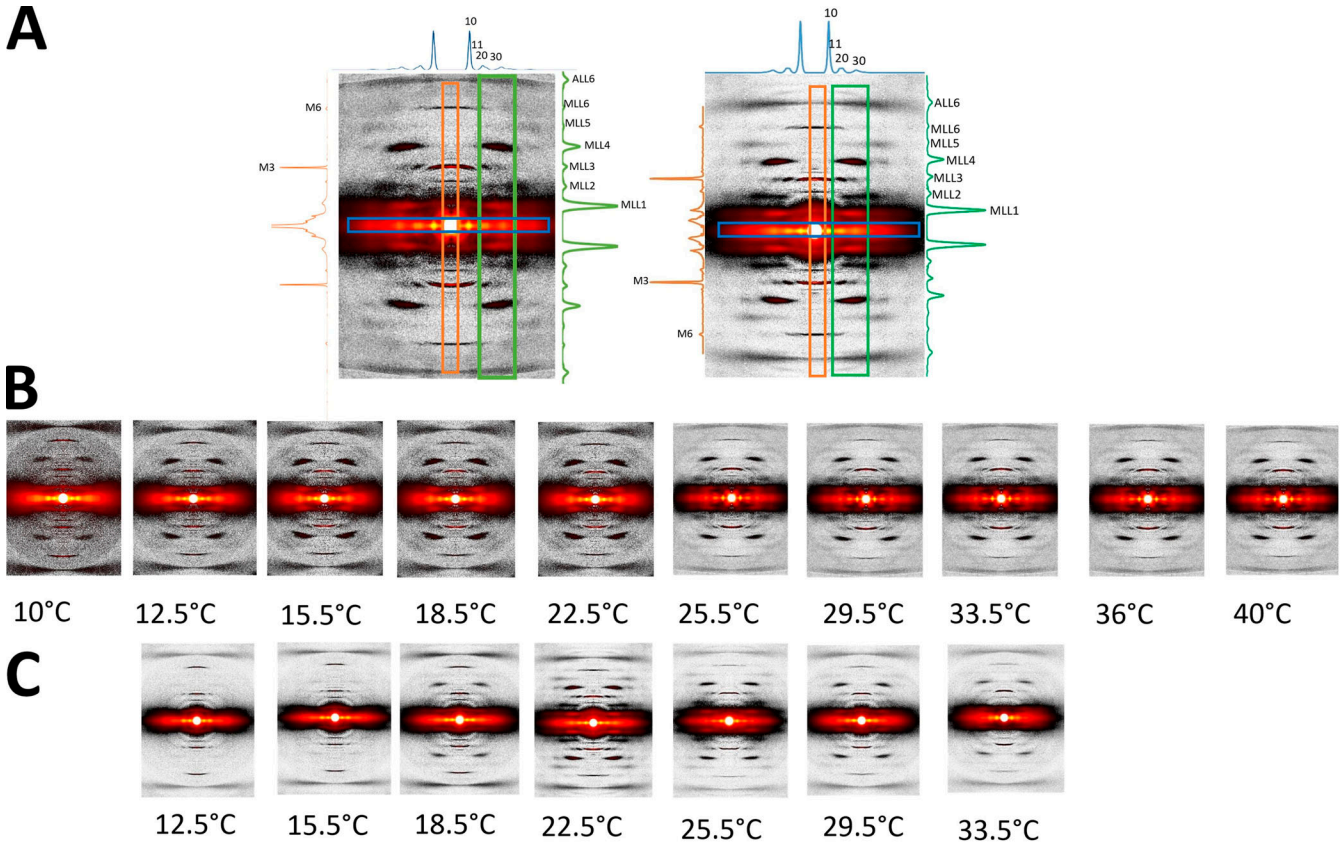


Figure 2. **XRD patterns from tarantula skeletal muscle. (A)** Relaxed muscles of an ex vivo leg (left) and an isolated live muscle (right), recorded at 22.5°C. Equatorial, meridional, and off-meridional intensity profiles (as shown in the corresponding colored boxes) are seen in blue (top), orange (left), and green (right), respectively. The axial span of the blue box in the equator is ±0.00755 $nm^{-1}$; the radial span of the orange box in the meridian is ±0.0081 $nm^{-1}$; and the green box radial range span is from 0.038 $nm^{-1}$ to 0.072 $nm^{-1}$. **(B and C)** XRD patterns of relaxed ex vivo leg muscles (B) and isolated muscles (C) recorded from 10°C to 40°C.

### Limitations

#### *Temperature measurement*

A limitation of the whole-femur experiments was that the thermocouple recorded the surrounding solution temperature rather than the temperature of the muscle inside the exoskeleton, but the muscle temperature should be closely correlated to the surrounding solution temperature. This problem was avoided for single isolated muscles.

#### *Radiation damage*

Radiation damage could affect the quality of our x-ray patterns and the physiological response. Radiation damage was minimized by (1) allowing a 10-ms rest period between each frame and (2) oscillating the samples continuously in the x-ray beam in a 2-D raster pattern at 10 mm/s. We recorded patterns at the starting temperature of 22.5°C and took patterns at this temperature again after cooling and after heating to check reversibility. Significant radiation damage would be manifested qualitatively as deterioration of the later 22.5°C patterns compared with the starting pattern. This was not observed in our experiments. Radiation damage was also minimized during the multiple exposures by recording only up to MLL6 and actin layer line 6 (ALL6).

#### *Sarcomere length*

Measurement of sarcomere length using laser diffraction in the muscles in the excised legs was not possible because the chitin exoskeleton is opaque to a laser beam. The sarcomere length, therefore, is unknown. To ensure consistency, the experiments were done keeping the angle of the femur with the tibia approximately as it is after excising the leg (i.e., approximately perpendicular). For the isolated muscle experiments, care was taken not to stretch the muscles during dissection to maintain rest length.

### Atomic modeling

We used USCF Chimera version 1.14 and its MatchMaker tool (Pettersen et al., 2004) for comparing the Protein Data Bank (PDB) structures in Fig. 1 B and Fig. 7.

### Online supplemental material

Video 1 depicts dissection details of the flexor femoris cbensis muscle of *A. hentzi*.

## Results

We studied the XRD pattern of skeletal muscles in the intact tarantula femur (i.e., with surrounding exoskeleton), which we term ex vivo, as well as in single isolated muscles (Fig. 2 A). The patterns were very similar, exhibiting six MLLs (MLL1–MLL6) and one ALL (ALL6), as described previously (Padrón et al., 2020). Therefore, we pooled the results of the two preparations. We

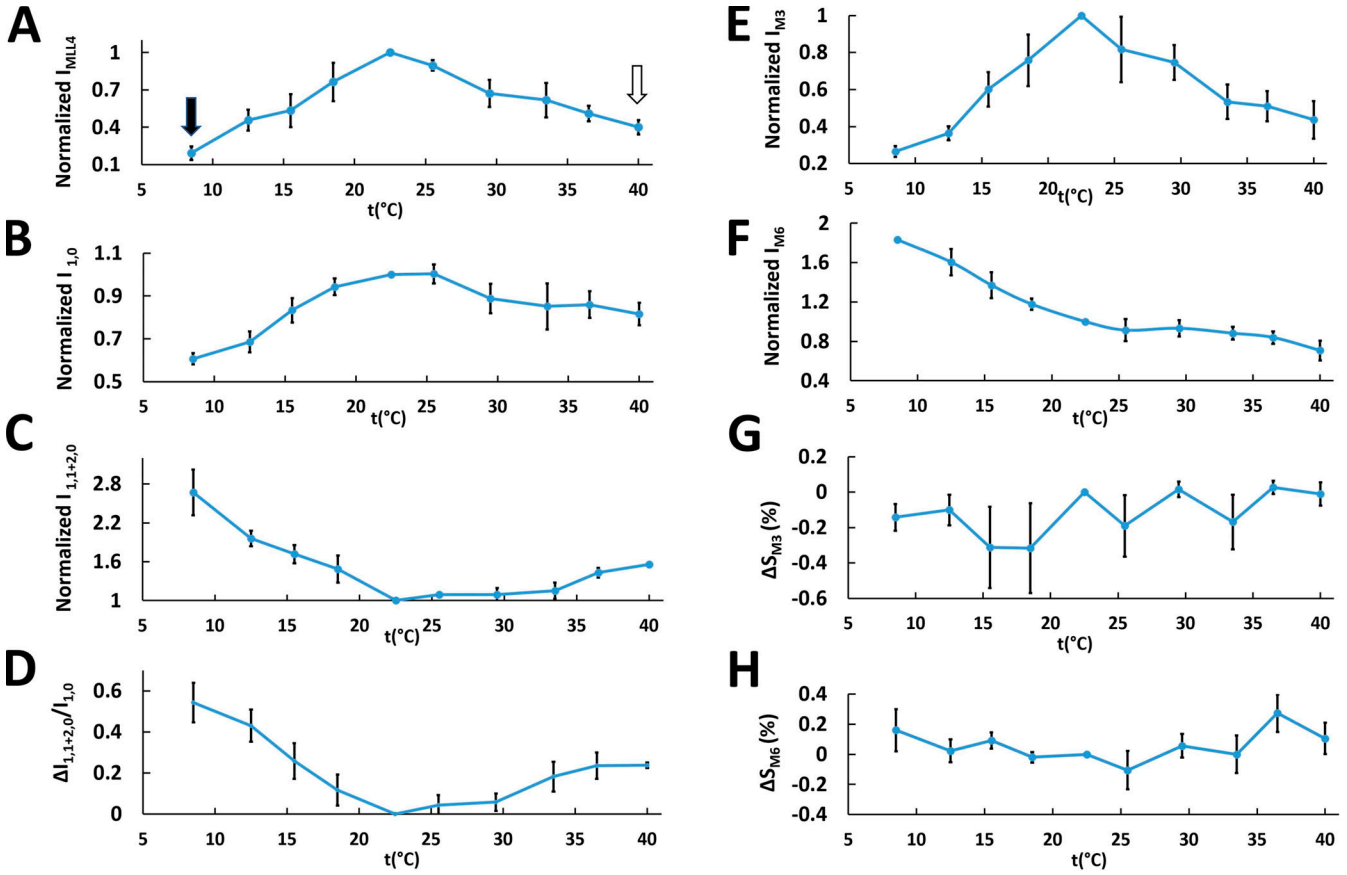


Figure 3. **Variation of the intensities of layer lines and meridional and equatorial reflections and their spacings in live relaxed tarantula skeletal muscle with temperatures (t) from 8.5°C to 40°C. (A)** Normalized $I_{MLL4}$. **(B–D)** Normalized $I_{1,0}$ (B) and $I_{1,1+2,0}$ (C) and the change of the $I_{1,1+2,0}/I_{1,0}$ ratio $\Delta I_{1,1+2,0}/I_{1,0}$ (D). **(E–H)** Normalized intensities of the third (E) and sixth (F) meridional reflections (M3 and M6, respectively) and their relative spacing changes (G and H). The residual values of $I_{MLL4}$ are shown in A with black (20%) and white (40%) arrows. The average value and its SEM is shown for each measurement at each temperature. Normalization was against values measured at 22.5°C. The results are given as mean ± SEM.

explored the changes in the XRD pattern of relaxed ex vivo (Fig. 2 B) and isolated (Fig. 2 C) muscles in the temperature range ~8.5–40°C.

For the equatorial reflections, the 1,0 intensity, $I_{1,0}$, was constant between 18°C and 25°C (Fig. 3 B) but decreased at temperatures outside this range; the intensity of the combined 1,1 and 2,0 equatorial reflections, $I_{1,1+2,0}$, was constant between 22°C and 34°C but increased below 21°C and above 34°C (Fig. 3 C). The $I_{1,1+2,0}/I_{1,0}$ ratio, a measure of the proximity of myosin heads to actin (Shimomura et al., 2016), was constant between 18°C and 29°C, increasing on either side of this range (Fig. 3 D) but midway on the high temperature side. These results suggest that at 22.5°C the heads are close to the backbone (high $I_{1,0}$, low $I_{1,1+2,0}$, low $\Delta I_{1,1+2,0}/I_{1,0}$), while at low temperature they move progressively away (low $I_{1,0}$, high $I_{1,1+2,0}$, high $\Delta I_{1,1+2,0}/I_{1,0}$). At high temperatures, a similar outward movement plateaus at a distance in the middle of the range seen for lowered temperatures (middle values for $I_{1,0}$, $I_{1,1+2,0}$, and $\Delta I_{1,1+2,0}/I_{1,0}$).

For the MLLs, MLL1–6 were very intense at 22.5°C in both ex vivo and isolated muscles, suggesting that the heads were helically ordered. In contrast, at both higher and lower temperatures, the layer lines became weaker (Fig. 2, B and C), more so for the lower temperatures ($I_{MLL1-6}$; Fig. 3 A and Fig. 4, A and B), while the intensity of the sixth-order ALL, $I_{ALL6}$, remained approximately constant (Fig. 4, A and B). We interpret the presence of an ~20% and ~40% residual $I_{MLL4}$ at the extreme temperatures of 8.5°C and 40°C, respectively (Fig. 3 A, black and white arrows, respectively), in a similar way to previous studies, where ~20–25% residual $I_{MLL1}$ intensity in contracting muscle was attributed to ~50% of heads remaining ordered in their helical positions, while 50% are disordered in the frog (Huxley et al., 1982; Tanaka et al., 1986) and the mouse (Ma et al., 2018a). In similar studies on contracting tarantula skeletal muscle (Padrón et al., 2020), where we have detailed information on the organization of BHs and FHs (Woodhead et al., 2005; Alamo et al., 2008; Alamo et al., 2016), simulation results for $I_{MLL1}$ and $I_{MLL4}$ showed residual values of ~34% and 14%, respectively, when all FHs were removed (equivalent to disorder), while all BHs were still present. Our interpretation suggested that the residual $I_{MLL1}$ and $I_{MLL4}$ came from the (more stable) BH helices, while the FHs were disordered during a tetanus. On the basis of these simulations, we suggest here that, at low temperature ($I_{MLL4}$ residual 20%; Fig. 3 A, black arrow), most BHs remain ordered and ~80% of FHs are disordered, while at high temperature ($I_{MLL4}$ residual 40%; Fig. 3 A, white arrow), most BHs remain ordered and ~50% of FHs remain ordered (Fig. 3, A–D).

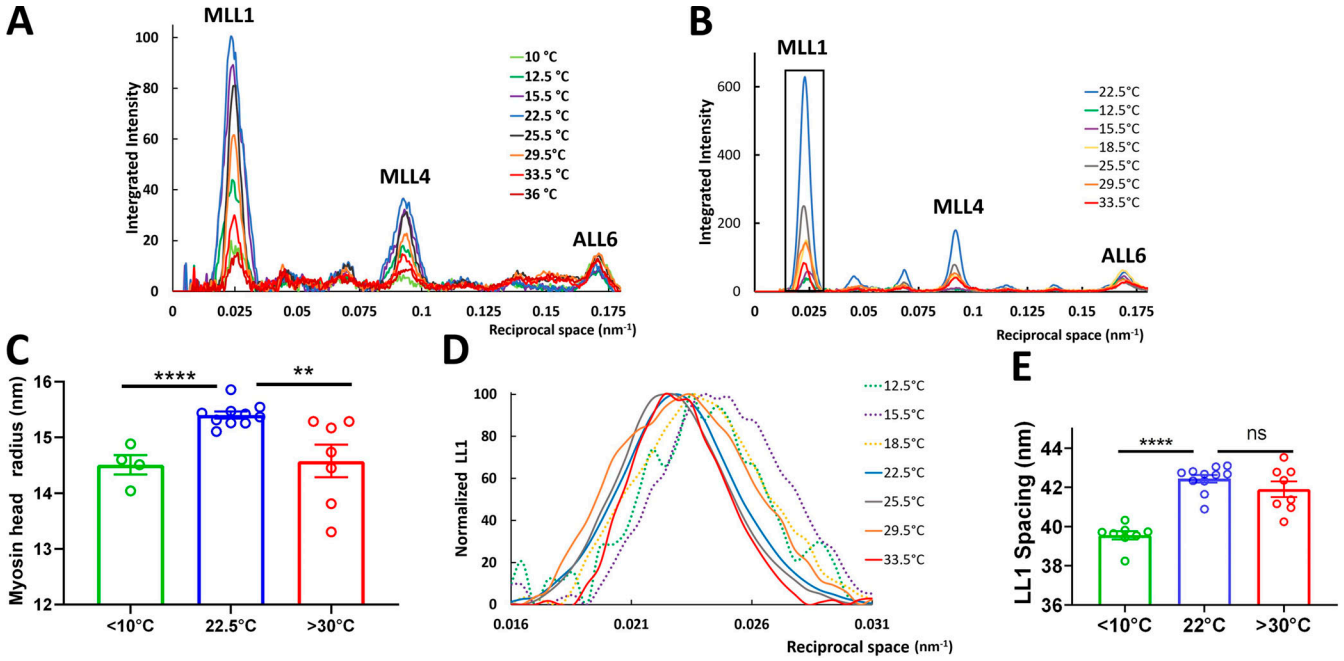


Figure 4. **Intensities of off-meridional layer lines from XRD patterns of relaxed tarantula skeletal muscle.** Integration area shown in Fig. 2 A, green box. **(A and B)** Example intensity traces from leg muscles in one leg ex vivo (A) and isolated live muscle (B). **(C)** Myosin head radius calculated from MLL4 profiles for temperatures <10°C, 22.5°C, and >30°C. **(D)** Normalized off-meridional axial profiles of the first MLL (LL1) parallel to meridian (boxed area in B), showing a shift of the first peak only at low temperature. **(E)** Peak LL1 spacings of the MLL1 profiles shown in D for temperatures <10°C, 22.5°C, and >30°C. The results are given as mean ± SEM. ns, not significant; **, P < 0.01; ****, P < 0.0001; two-tailed unpaired Student's *t* tests.

The average radius, r, of the heads (BHs and FHs combined) at <10°C, 22.5°C, and >30°C was calculated from the MLL4 intensity profiles, assuming a $J_4$ Bessel function, the first maximum of which occurs when the argument $2\pi Rr$ is equal to 5.3176 [i.e., $J_4(2\pi Rr) = 5.3176$]. Comparison of the radial position of the MLL4 maxima for these temperatures (Fig. 4 C) shows that the average radii of the BHs and FHs combined is 15.5 nm at 22.5°C (helices of BHs and FHs in Fig. 1 C, a), ∼1.0 nm greater than the average (14.5 nm) at <10°C (most FHs disordered and BHs ordered) and >30°C (∼50% FHs disordered, BHs ordered; Fig. 1 C, b). This is consistent with disordering of the FHs (which are at higher initial radius; Fig. 1 C, a) as temperature varies up or down from 22.5°C, while the lower-radius BHs remain more ordered. Our previous simulation results (Padrón et al., 2020) showed that the progressive removal of FHs (simulating disordering) induced a progressive decrease of MLL4 intensity, with a concomitant shifting of the MLL4 peak to higher angles, away from the meridian, exactly as we observed here with change in temperature from 22.5°C (Fig. 4 C). This supports our interpretation of temperature-induced disordering of the FHs, while the BHs, at lower radius, remain more ordered.

The first order of the myosin-based layer line (MLL1; Fig. 4 D) shows that the behavior of the heads is different at low and high temperatures. At lower temperatures, the intensity of MLL1 ($I_{MLL1}$) decreases (Fig. 4, A and B). At the same time, the axial position of the peak intensity shifts to slightly higher angles (see enlargement of the boxed region in Fig. 4 B, shown in Fig. 4 D). This apparent shift in spacing is most likely due to mixing of the first MLL (MLL1; ∼43.5 nm) with the first ALL (ALL1; ∼38 nm), as the two become comparable in intensity at the lower temperatures, so that the combined intensity peak appears to be shifted to higher angles axially. At higher temperature, the peak MLL1 intensity decreases (Fig. 4, A and B) but remains at the same spacing; in this case, the decrease in MLL1 intensity is less, and it therefore mixes less with the ALL1 (Fig. 4 E). The peak shift at lower but not higher temperatures is consistent with disordering of FHs at low temperature.

The intensities of the myosin meridional reflections, both ex vivo and isolated, also decreased as temperature varied above and below 22.5°C (Fig. 5, A and B). The third-order reflection intensity, $I_{M3}$, decreased substantially below 18°C and above 25°C (Fig. 3 E), while the sixth-order reflection intensity, $I_{M6}$, decreased linearly between 8.5°C and 40°C (Fig. 3 F). There were no systematic changes of the spacings of the M3 and M6 reflections ($S_{M3}$ and $S_{M6}$; Fig. 3, G and H), suggesting that the periodicity of myosin heads and backbone packing were insensitive to temperature change. This differs from the mouse, in which $S_{M3}$ is constant with temperature, while there is a small increase of $S_{M6}$ at low temperature (Caremani et al., 2019). The radial width of the M3 reflection did not change significantly at low temperature (Fig. 5, C–E), even though $I_{M3}$ decreased substantially. In the mouse, the M3 width was also independent of temperature (Caremani et al., 2019). The radial width of the M3 reflection is a function of the degree of axial registration of the thick filaments relative to each other, with decreases in axial ordering leading to increases in radial width (Huxley et al., 1982). The decrease of $I_{M3}$ appears to be greater at 12.5°C than

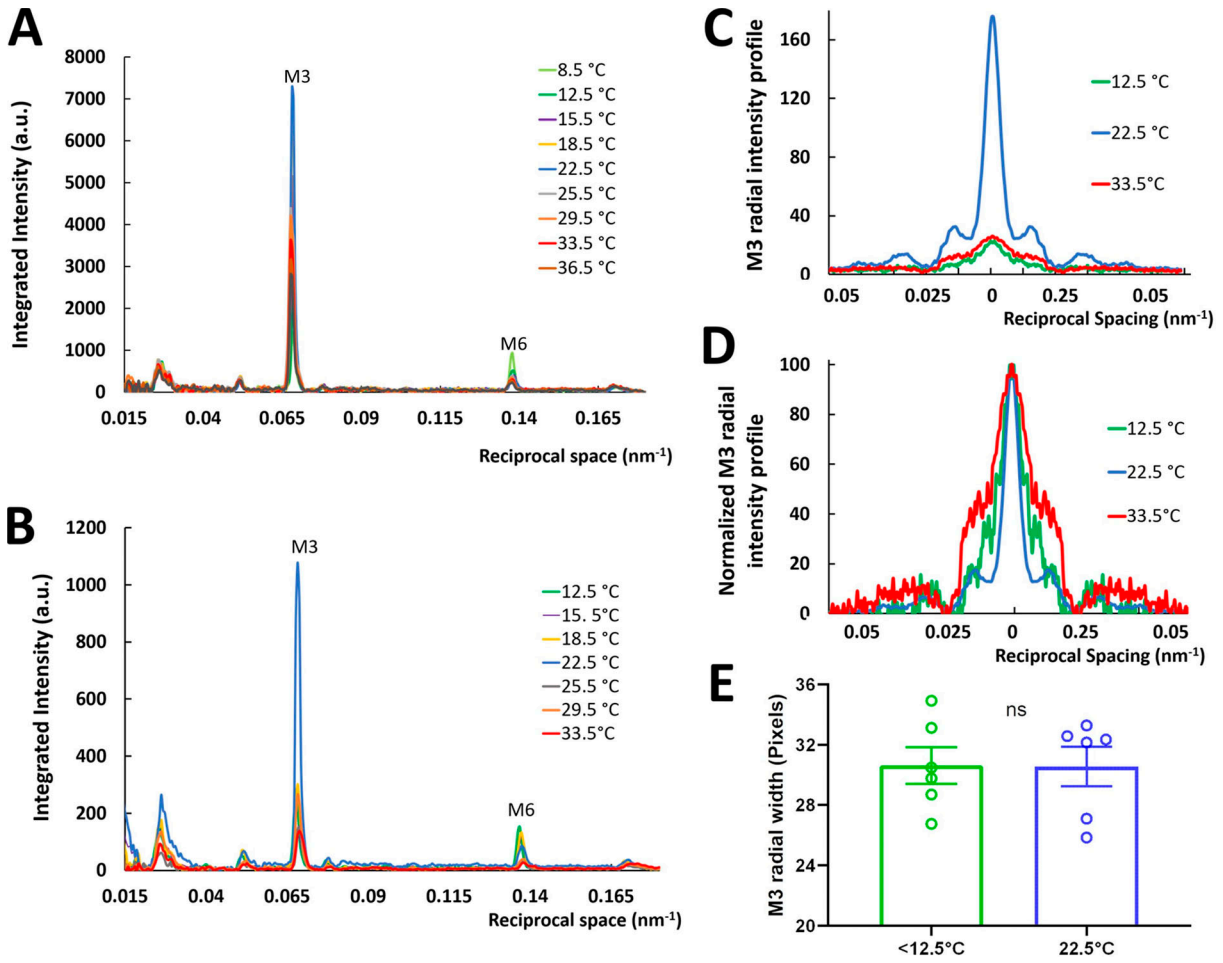


Figure 5. **Intensity of reflections along the meridian from XRD patterns of relaxed tarantula skeletal muscle.** Integrated area seen in Fig. 2 A, orange box. **(A and B)** Ex vivo leg muscles (A) and isolated live muscle (B). **(C and D)** Radial intensity profile of the third myosin reflection M3 (C) and normalized (D) at <12.5°C, 22.5°C, and >33.5°C. **(E)** Radial width of the M3 reflection for <12.5°C and 22.5°C. The results are given as mean ± SEM. ns, not significant.

at 33.5°C (Fig. 3 E), in agreement with the disorder ascribed to the FHs at low and high temperature.

These layer line and equatorial intensity changes, taken together, suggest that the myosin heads of relaxed tarantula skeletal muscle thick filaments are thermosensitive. At 22.5°C, the heads (BHs and FHs) are close to the backbone and helically organized (Fig. 1 A, a). At low temperature, most FHs disorder and move away from the backbone, while the BHs remain helically ordered. At high temperature, half of the FHs become disordered and move away semipermanently to a location midway to the thin filaments, and the other half remain docked as swaying heads, while the BHs remain close to the backbone and helically ordered.

## Discussion

### Changes in the XRD pattern with temperature can be explained by the dynamics of the BHs and FHs

Our results show that there is an optimum range of temperature, between 20°C and 27.5°C, for helical order in the thick filaments of live tarantula skeletal muscle (Fig. 6 A, yellow box) and that both higher and lower temperatures induce disorder and movement of the heads away from the backbone. Disordering at lower temperatures has been observed in previous studies (of mammalian muscle), but not at higher temperatures. These studies were interpreted in terms of disordering of the heads as a whole (Malinchik et al., 1997; Xu et al., 1999; Xu et al., 2003; Wray, J.S. 1987. Structure of relaxed myosin filaments in relation to nucleotide state in vertebrate skeletal muscle. J. Muscle Res. Cell Motil. 8:62). Here, we suggest an interpretation of the temperature-induced changes in tarantula skeletal muscle thick filaments in terms of different behaviors of the BH and FH helices (Fig. 1 C, a and b). This follows our approach in analyzing changes in the tarantula skeletal muscle XRD pattern upon activation in terms of the BH and FH heads (Padrón et al., 2020). Our interpretation incorporates the observation that helical order requires a bent conformation of the head (as seen in cryo-EM reconstructions of tarantula skeletal muscle thick filaments; Woodhead et al., 2005; Alamo et al., 2008), in which the lever arm is in the "up" position, and switch II and the γ-phosphate pocket are "closed," allowing the heads to form the IHM structure, while disorder is induced by the straight conformation, in which the lever arm is "down" and switch II and the γ-phosphate pocket

are "open" (Xu et al., 1999; Xu et al., 2003; Zoghbi et al., 2004), which cannot form the IHM.

We propose the following model, in terms of BHs and FHs (Fig. 6 B), to explain the structural changes in the thick filaments (Figs. 2 and 3) with change in temperature. At the $t_{op}$ range ($20°C < t_{op} < 27.5°C$), the MLLs are the most intense (Figs. 2; 3; 4, A and B; 5, A and B; and 6 A), consistent with organization of the BHs and FHs in two coaxial helices, with the BHs closer to the filament backbone than the FHs (Fig. 1 C, a; and Fig. 6 B, c), as demonstrated by cryo-EM of relaxed thick filaments (Woodhead et al., 2005; Alamo et al., 2008; Alamo et al., 2016). This is the arrangement we previously demonstrated also in intact (in vivo and ex vivo) relaxed tarantula skeletal muscle by modeling the XRD pattern and comparing it with the cryo-EM 3-D reconstruction (Padrón et al., 2020).

We propose that in the $t_{op}$ range (Fig. 6 A, yellow box), all heads have the bent conformation (containing Mg.ADP.$P_i$) and thus form IHM helices (Fig. 6 B, c), as found by XRD and EM. When temperature decreases below $t_{op}$, the heads progressively transition to the straight conformation and thus to the Mg.ATP state, causing them to break their IHM interactions, move away from the filament backbone, and become disordered (Fig. 6 B, b to a), as observed with mammalian muscle (Xu et al., 1999; Xu et al., 2003). We suggest that it is the heads with the slow turnover rate (the docked swaying FHs; Fig. 6 B, b to a) that undergo this transition, while the heads with a very slow turnover rate (the docked BHs) remain helically ordered (Fig. 6 B, b to a). We propose that, when temperature increases above $t_{op}$ (Fig. 6 B, d to e), the heads remain in the Mg.ADP.$P_i$ state, and a fraction of the FHs become progressively disordered, located semipermanently at a distance midway to the thin filaments, and the remaining FHs remain docked as swaying heads, while the BHs remain helically ordered (explaining the stronger residual MLL intensities at high temperature compared with low temperature; Fig. 6 A, white arrow versus black arrow) close to the thick-filament backbone.

The exact mechanism by which temperature changes affect the shape of the heads (bent or straight), and thus stability of the IHM and helical ordering, remains uncertain. In addition to its effect on the ADP.$P_i$ ⇔ ATP equilibrium, temperature also affects electrostatic and hydrophobic interactions, which could impact the stability of the IHM conformation, held together by specific FH–BH and BH–S2 interactions as well as between both regulatory light chains (Alamo et al., 2016). The forces in electrostatic interactions in water are given by Coulomb's law, $F = (q_1q_2)/4\pi\varepsilon r^2$, which involves the water dielectric constant ε, shown for proteins to be temperature dependent, varying from protein to protein, and decreasing when temperature increases (Christen et al., 1996); thus, 1/ε increases with temperature, and with it the electrostatic force. The hydrophobic force becomes weaker at both lower and higher temperatures (van Dijk et al., 2015). Further work is needed to understand the effect of temperature on the hydrolysis equilibrium, the conformations of the heads, and the stability of the IHM conformation.

Taken together, the results for $I_{MLL4}$ (Fig. 3 A; Fig. 4, A and B; and Fig. 6 A), the radial spacing of MLL4 peaks (Fig. 4 C), and the axial spacing of the MLL1 (Fig. 4 D) suggest that at $t_{op}$ the heads are organized into two helices, the BH helices and FH helices, respectively (Fig. 6 B, c). Lowering the temperature below $t_{op}$ progressively disorders the FH but not the BH helices (Fig. 6 B, c to a), while increasing the temperature above $t_{op}$ disorders part of the FHs, whereas the BHs remain ordered, forming helices (Fig. 6 B, c–e). This interpretation is supported by the asymmetric changes of $I_{1,0}$, $I_{1,1+2,0}$, and their ratio below and above $t_{op}$ (Fig. 3, B–D; and Fig. 6 A): Below $t_{op}$, the average position of the heads (BHs and FHs combined) progressively moves away from the backbone (Fig. 6, A and B, c to a), due primarily to movement of the FHs, whereas above $t_{op}$, a fraction of the FHs disorder and move away, remaining semipermanently at a midway distance to the thin filaments, and the rest of docked FHs remain swaying while BHs remain forming helices (Fig. 6 B, e)

### There are two distinct energy-saving mechanisms in relaxed tarantula skeletal muscle

We interpret our results in the context of the cross-bridge cycle proposed using scallop myosin head crystal structures in different nucleotide states (Robert-Paganin et al., 2020) by comparison with the tarantula skeletal muscle myosin head structures (Fig. 7). The FHs in relaxed muscle can detach briefly, swaying back and forth briefly from their docked, helical IHM positions (Fig. 7 A; Brito et al., 2011; Sulbarán et al., 2013; Alamo et al., 2016; Sulbarán et al., 2020) due to thermal fluctuations. The swaying FHs have the prepower stroke, bent structure (PDB accession no. 3JBH; Fig. 1 A; determined by cryo-EM; Woodhead et al., 2005; Alamo et al., 2008; Alamo et al., 2016), similar to the PDB accession no. 1QVI prepower stroke (Fig. 1 B) of scallop muscle included in the cycle of Robert-Paganin et al. (2020); Fig. 7, step 1, showing comparison of the FH of PDB 3JBH with PDB 1QVI). These swaying (bent) heads can weakly attach to the switched-off thin filaments (Fig. 7, step 2). When the thin filament is switched on by the tropomyosin/troponin $Ca^{2+}$-activation mechanism, present in tarantula skeletal muscle (Craig and Lehman, 2001), tension and displacement are produced by the power stroke (Fig. 7, step 3). As part of this process, $P_i$ is released, followed by Mg.ADP, leading to the rigor structure (Fig. 7, step 4). The binding of Mg.ATP produces fast dissociation of the rigor head to a straight, Mg.ATP-containing postrigor head (Fig. 7, step 5). This is followed by fast ATP hydrolysis and the recovery stroke (Fig. 7, step 6), in which the head is primed to the prepower stroke bent structure, capable of weakly binding to actin (Fig. 7, step 1).

This cycle suggests two different types of mechanisms by which energy (ATP) may be conserved in relaxed tarantula skeletal muscle. (1) Over the $t_{op}$ range ($20°C < t_{op} < 27.5°C$), ADP.$P_i$ is bound to the bent heads forming the helically arranged IHM; the docked BHs and FHs docked onto BHs and the swaying FHs are in a superrelaxed (SRX) energy-saving state (Stewart et al., 2010; Cooke, 2011) as shown by the very slow turnover rates (docked BHs) and slow turnover rates (docked FHs onto BHs) in tarantula skeletal muscle (Fig. 7 A; Naber et al., 2011; Alamo et al., 2016). (2) At low temperatures (<20°C), disordered heads in their straight conformation (probably with Mg.ATP bound, based on vertebrate data; Xu et al., 1999; Xu et al., 2003) are in the ATP state and are thus inhibited from going through the ATPase cycle or binding to actin, thereby saving ATP (Fig. 7 B), similar to the refractory state proposed in mouse skeletal muscle at low temperature (Caremani et al., 2019).

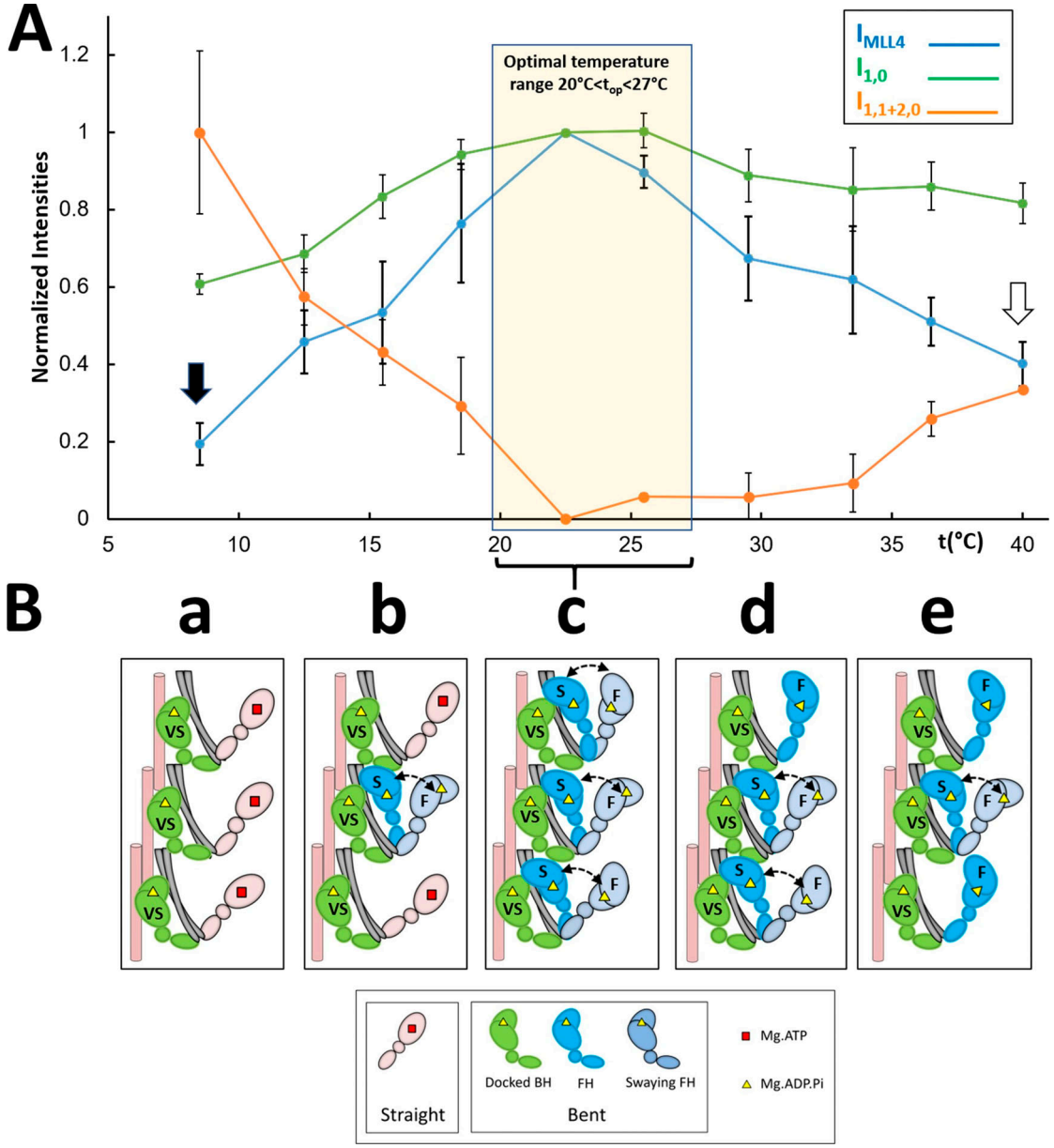


Figure 6. **Proposed thermosensing mechanism for thick filaments of relaxed tarantula skeletal muscle. (A)** Normalized $I_{MLL4}$, $I_{1,0}$, and $I_{1,1+2,0}$ (from Fig. 3, A–C). The residual values of $I_{MLL4}$ are shown with black (20%) and white (40%) arrows. **(B)** Proposed thermosensing mechanism. (c) At the $t_{op}$ range 20–27.5°C, the BHs (green) and FHs (blue) exhibit the bent structure required to form IHMs and helices. The FHs can sway away (light gray head, double arrow) and back, docking on their partner BH IHM positions. Lowering the temperature from this $t_{op}$ range (b to a) progressively changes the heads to the straight structure (pink heads), incapable of making IHMs, and thus becoming disordered, which occurs in the FHs with slow (S) turnover rates, while the BHs with a very slow (VS) turnover rate remain ordered (c to b). We propose that progressively increasing temperature from the $t_{op}$ range affects only a fraction of the FHs, which become semi-permanently disordered midway to the thin filaments, while the BHs remain ordered (c to e; see text). The very slow (>1,800 s), slow (250–300 s), and fast (<30 s) ATP turnover rates measured in relaxed tarantula skeletal muscle thick filaments (Naber et al., 2011), associated with the docked BHs, docked FHs onto BHs, and released FHs, are marked in the heads as VS, S, and F, respectively (Alamo et al., 2016; see text). The results are given as mean ± SEM.

In tarantula skeletal muscle, these SRX and refractory energy-saving mechanisms (Fig. 7, A and B) could conserve ATP over a wide temperature range: the very slow ATP turnover rate of the docked BHs is present at all temperatures explored here (8.5–40°C), while the refractory effect, in the FHs, occurs only below 20°C. At higher temperatures, we propose that the disordered, semipermanently detached FHs midway to the thin filaments are in the bent, ADP.$P_i$ state, primed for rapid interaction with actin; these may be comparable to the disordered heads that lead to rapid force development following tetanic stimulation (Padrón et al., 2020), but in this case without regulatory light chain phosphorylation.

### Response to variable temperature in tarantula is like other ectotherms

Locomotion, feeding, growth, reproduction, and survival of animals all depend on body temperature (Kingsolver and Buckley, 2017), as summarized in thermal curves in which performance

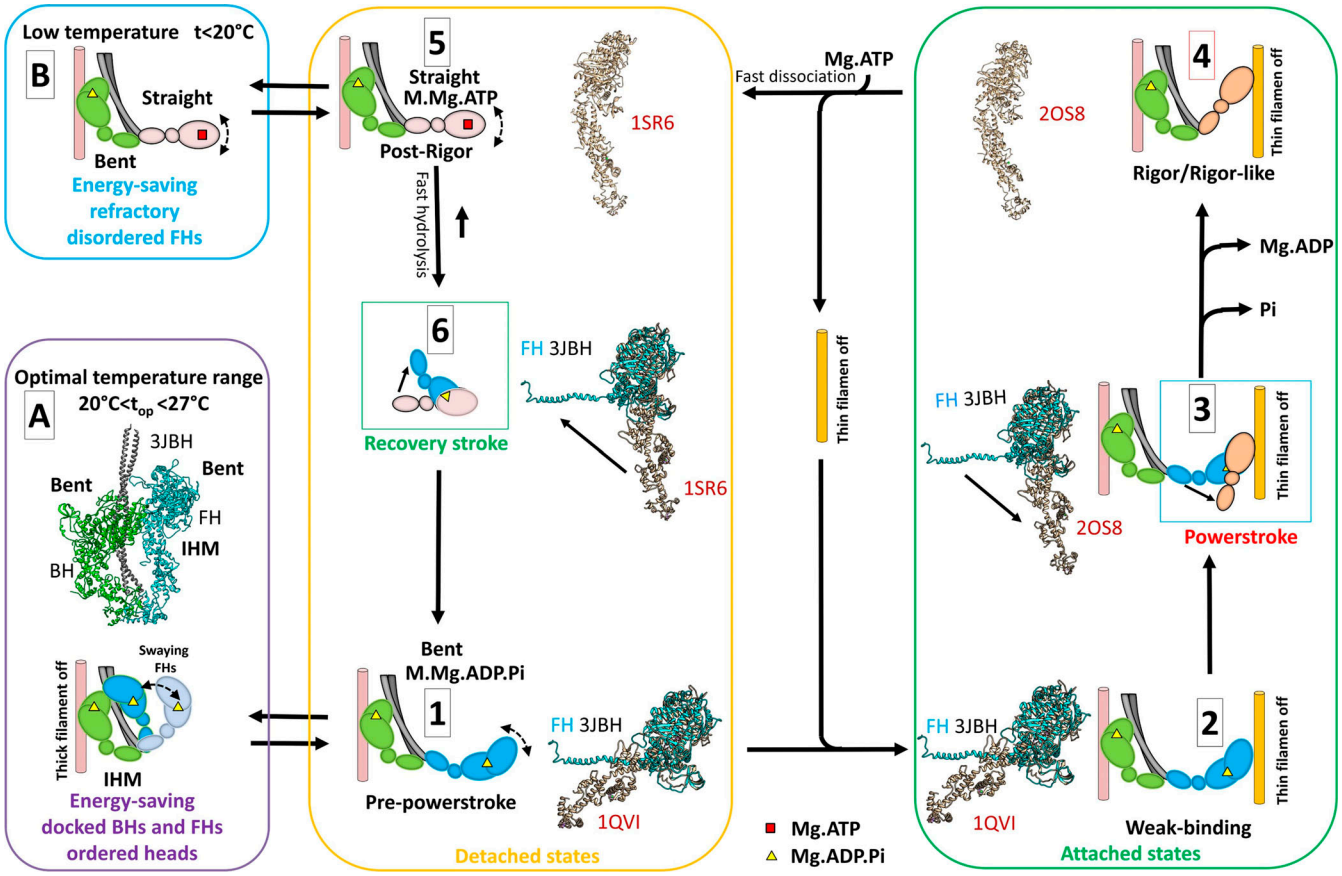


Figure 7. **Two ATP energy-saving mechanisms proposed in tarantula skeletal muscle.** A cross-bridge cycle for tarantula skeletal muscle, based on previous work by Robert-Paganin et al. (2020), is shown and includes actin-detached steps (yellow box) and actin-attached steps (green box). **(A)** The energy-saving IHM (PDB accession no. 3JBH) allows quick incorporation of the detached, swaying FHs to the cycle (Padrón et al., 2020). The FHs, which are in the bent, prepower stroke structure (similar to PDB accession no. 1QVI, shown in tan in steps 1 and 2 and in Fig. 1 B) containing Mg.ADP.$P_i$ (Zoghbi et al., 2004), can sway away and back by Brownian motion (Brito et al., 2011; step 1) and weakly attach to the switched-off thin filaments (step 2). When the thin filament is switched on by the tropomyosin/troponin $Ca^{2+}$ switch (Craig and Lehman, 2001), the FHs attach strongly, going through the power stroke and producing force and displacement (step 3) transitioning, after $P_i$ and then ADP release, to a nucleotide-free rigor/rigor-like structure similar to PDB accession no. 2OS8 (step 4). The binding of Mg.ATP to the rigor/rigor-like FHs induces fast dissociation of the heads from actin (step 5), followed by a rapid hydrolysis of Mg.ATP to Mg.ADP.$P_i$ during the recovery stroke (step 6), reproducing the prepower stroke (step 1). We propose that there are two different mechanisms for ATP energy saving in the relaxed, detached states involving (1) IHM energy saving by helically ordered docked BHs and FHs, with swaying FHs enabled to quickly produce force as they are all in the bent prepower stroke Mg.ADP.$P_i$-containing state (A, purple box); and (2) the refractory, energy-saving, disordered, and functionally disabled heads that need to be reprimed during the recovery stroke to achieve the prepower stroke, enabling them to produce force (B, blue box). The structures in steps 1–3 and 6 show the superimposition of the motor domains of the FH of PDB 3JBH in the same orientation (without the regulatory and essential light chains) with the crystal structures PDB 1QVI, PDB 2SO8, and PDB 1SR6.

increases with temperature, reaching a maximum at an intermediate $t_{op}$ and decreasing with further temperature increase (Huey and Kingsolver, 1989). The shape of these thermal performance curves reflects the effect of temperature on the rate of enzymatic processes and on enzyme activation and stability at high temperatures (Ratkowsky et al., 2005).

Tarantulas, like all ectotherms, are unable to regulate their temperatures internally. Their muscles are thus potentially subject to a wide range of surrounding temperatures (from −4°C to 47°C in the case of the *A. hentzi* we studied here). They avoid temperature extremes during winter and summer by sheltering in insulated burrows, which moderates external temperature influence and would keep their muscles closer to $t_{op}$ (Fig. 6 B, c), conserving energy by SRX (as well as on the wider −4°C to 47°C range), becoming dormant and saving energy at lower temperatures by the refractory mechanism (Fig. 6 B, a), while at higher temperatures, the semipermanently detached disordered FHs (Fig. 6 B, e) could lead to rapid force development similarly to the disordered heads following tetanic stimulation (Padrón et al., 2020). As ectotherms, use of internal physiological sources to control their body temperature is negligible. Energy from food is not used by tarantulas to control their body temperature, but mostly for moving, despite their remaining stationary most of the time.

The surrounding temperature determines the tarantula body and muscle temperature. Optimal $t_{op}$ and survival temperature ranges in ectotherms such as tarantulas are much wider than in homeotherms because tarantulas need to be able to endure quick equilibration of their bodies to the extreme annual low and high temperatures in their habitats. XRD and EM have shown that

there is a range of $t_{op}$ values in which thick filaments are helically ordered, depending on species. For homeothermic animals, such as mammals including the rabbit (Kensler et al., 1994; Wray, J.S. 1987. Structure of relaxed myosin filaments in relation to nucleotide state in vertebrate skeletal muscle. J. Muscle Res. Cell Motil. 8:62) and mouse (Caremani et al., 2019), this optimal, physiologically controlled, range is >30°C, and >25°C in the chicken (Kensler and Woodhead, 1995; i.e., close to the in vivo regulated body temperature in these animals [rabbit, 36.6–38.9°C; mouse, 36.5–38°C; chicken, 40.6–41.7°C]), with thick filaments becoming disordered at lower temperatures. For ectotherms, such as the tarantula, the optimal range shifts to 20–27.5°C, with disordering outside this range, while for other ectotherms, such as the goldfish (Kensler et al., 1994) and frog (Huxley and Brown, 1967), the optimal range seems to be much broader (4–25°C). Thus, in broad terms, helical ordering of the myosin heads correlates with the normal physiological temperature range of these diverse animals, suggesting that it is important for normal muscle function.

## Acknowledgments

Henk L. Granzier served as editor.

We thank Lic. Lorenzo Alamo for his help with Fig. 1 C and Dr. Pura Bolaños for recording Video 1.

This research was supported in part by National Institutes of Health grants R01AR072036 (to R. Craig), R01AR067279 (to R. Craig and D. Warshaw), and R01HL139883 (to R. Craig and R. Moss), and used resources of the Advanced Photon Source, a U.S. Department of Energy Office of Science user facility operated by Argonne National Laboratory under contract DE-AC02-06CH11357. Use of the BioCAT Beamline 18ID was supported by National Institute of General Medical Sciences grant P41 GM103622. Use of the Pilatus 3 1M detector was provided by National Institute of General Medical Sciences grant 1S10OD018090-01. Molecular graphics and analyses were performed with UCSF Chimera, developed by the Resource for Biocomputing, Visualization, and Informatics at the University of California, San Francisco, with support from National Institutes of Health grant P41-GM103311. The content of this work is solely the responsibility of the authors and does not necessarily reflect the official views of the National Institutes of Health.

The authors declare no competing financial interests.

Author contributions: W. Ma, S. Duno-Miranda, T. Irving, R. Craig, and R. Padrón designed and performed the research; W. Ma, T. Irving, and R. Padrón analyzed data; and W. Ma, T. Irving, R. Craig, and R. Padrón wrote the paper.

Submitted: 30 September 2020
Accepted: 22 December 2020

## References

Alamo, L., W. Wriggers, A. Pinto, F. Bártoli, L. Salazar, F.Q. Zhao, R. Craig, and R. Padrón. 2008. Three-dimensional reconstruction of tarantula myosin filaments suggests how phosphorylation may regulate myosin activity. *J. Mol. Biol.* 384:780–797. https://doi.org/10.1016/j.jmb.2008.10.013

Alamo, L., D. Qi, W. Wriggers, A. Pinto, J. Zhu, A. Bilbao, R.E. Gillilan, S. Hu, and R. Padrón. 2016. Conserved intramolecular interactions maintain myosin interacting-heads motifs explaining tarantula muscle super-relaxed state structural basis. *J. Mol. Biol.* 428:1142–1164. https://doi.org/10.1016/j.jmb.2016.01.027

Alamo, L., N. Koubassova, A. Pinto, R. Gillilan, A. Tsaturyan, and R. Padrón. 2017. Lessons from a tarantula: new insights into muscle thick filament and myosin interacting-heads motif structure and function. *Biophys. Rev.* 9:461–480. https://doi.org/10.1007/s12551-017-0295-1

Alamo, L., A. Pinto, G. Sulbarán, J. Mavárez, and R. Padrón. 2018. Lessons from a tarantula: new insights into myosin interacting-heads motif evolution and its implications on disease. *Biophys. Rev.* 10:1465–1477. https://doi.org/10.1007/s12551-017-0292-4

Brito, R., L. Alamo, U. Lundberg, J.R. Guerrero, A. Pinto, G. Sulbarán, M.A. Gawinowicz, R. Craig, and R. Padrón. 2011. A molecular model of phosphorylation-based activation and potentiation of tarantula muscle thick filaments. *J. Mol. Biol.* 414:44–61. https://doi.org/10.1016/j.jmb.2011.09.017

Caremani, M., E. Brunello, M. Linari, L. Fusi, T.C. Irving, D. Gore, G. Piazzesi, M. Irving, V. Lombardi, and M. Reconditi. 2019. Low temperature traps myosin motors of mammalian muscle in a refractory state that prevents activation. *J. Gen. Physiol.* 151:1272–1286. https://doi.org/10.1085/jgp.201912424

Christen, R.P., S.I. Nomikos, and E.T. Smith. 1996. Probing protein electrostatic interactions through temperature/reduction potential profiles. *J. Biol. Inorg. Chem.* 1:515–522. https://doi.org/10.1007/s007750050086

Cooke, R. 2011. The role of the myosin ATPase activity in adaptive thermogenesis by skeletal muscle. *Biophys. Rev.* 3:33–45. https://doi.org/10.1007/s12551-011-0044-9

Craig, R., and W. Lehman. 2001. Crossbridge and tropomyosin positions observed in native, interacting thick and thin filaments. *J. Mol. Biol.* 311:1027–1036. https://doi.org/10.1006/jmbi.2001.4897

Dillon, L. 1952. The myology of the araneid leg. *J. Morphol.* 90:467–480. https://doi.org/10.1002/jmor.1050900304

Fischetti, R., S. Stepanov, G. Rosenbaum, R. Barrea, E. Black, D. Gore, R. Heurich, E. Kondrashkina, A.J. Kropf, S. Wang, et al. 2004. The BioCAT undulator beamline 18ID: a facility for biological non-crystalline diffraction and X-ray absorption spectroscopy at the Advanced Photon Source. *J. Synchrotron Radiat.* 11:399–405. https://doi.org/10.1107/S0909049504016760

Gourinath, S., D.M. Himmel, J.H. Brown, L. Reshetnikova, A.G. Szent-Györgyi, and C. Cohen. 2003. Crystal structure of scallop Myosin s1 in the pre-power stroke state to 2.6 a resolution: flexibility and function in the head. *Structure.* 11:1621–1627. https://doi.org/10.1016/j.str.2003.10.013

Hammersley, A.P. 2016. FIT2D: a multi-purpose data reduction, analysis and visualization program. *J. Appl. Cryst.* 49:646–652. https://doi.org/10.1107/S1600576716000455

Huey, R.B., and J.G. Kingsolver. 1989. Evolution of thermal sensitivity of ectotherm performance. *Trends Ecol. Evol.* 4:131–135. https://doi.org/10.1016/0169-5347(89)90211-5

Huxley, H.E., and W. Brown. 1967. The low-angle x-ray diagram of vertebrate striated muscle and its behaviour during contraction and rigor. *J. Mol. Biol.* 30:383–434. https://doi.org/10.1016/S0022-2836(67)80046-9

Huxley, H.E., A.R. Faruqi, M. Kress, J. Bordas, and M.H. Koch. 1982. Time-resolved X-ray diffraction studies of the myosin layer-line reflections during muscle contraction. *J. Mol. Biol.* 158:637–684. https://doi.org/10.1016/0022-2836(82)90253-4

Jiratrakanvong, J., J. Shao, M. Menendez, X. Li, J. Li, W. Ma, G. Agam, and T. Irving. 2018. MuscleX: software suite for diffraction X-ray imaging V1.13.1. *Zenodo.* https://doi.org/10.5281/zenodo.1195050 (accessed July 28, 2020).

Kensler, R.W., and J.L. Woodhead. 1995. The chicken muscle thick filament: temperature and the relaxed cross-bridge arrangement. *J. Muscle Res. Cell Motil.* 16:79–90. https://doi.org/10.1007/BF00125312

Kensler, R.W., S. Peterson, and M. Norberg. 1994. The effects of changes in temperature or ionic strength on isolated rabbit and fish skeletal muscle thick filaments. *J. Muscle Res. Cell Motil.* 15:69–79. https://doi.org/10.1007/BF00123834

Kingsolver, J.G., and L.B. Buckley. 2017. Quantifying thermal extremes and biological variation to predict evolutionary responses to changing climate. *Philos. Trans. R. Soc. Lond. B Biol. Sci.* 372:20160147. https://doi.org/10.1098/rstb.2016.0147

Lee, K.H., G. Sulbarán, S. Yang, J.Y. Mun, L. Alamo, A. Pinto, O. Sato, M. Ikebe, X. Liu, E.D. Korn, et al. 2018. Interacting-heads motif has been conserved as a mechanism of myosin II inhibition since before the origin of animals. *Proc. Natl. Acad. Sci. USA.* 115:E1991–E2000. https://doi.org/10.1073/pnas.1715247115

Lewbart, G. 2012. Invertebrate Medicine. Second edition. John Wiley & Sons, Inc., Chichester, UK.

Ma, W., H. Gong, and T. Irving. 2018a. Myosin head configurations in resting and contracting murine skeletal muscle. *Int. J. Mol. Sci.* 19:2643. https://doi.org/10.3390/ijms19092643

Ma, W., H. Gong, B. Kiss, E.J. Lee, H. Granzier, and T. Irving. 2018b. Thick-filament extensibility in intact skeletal muscle. *Biophys. J.* 115: 1580–1588. https://doi.org/10.1016/j.bpj.2018.08.038

Malinchik, S., S. Xu, and L.C. Yu. 1997. Temperature-induced structural changes in the myosin thick filament of skinned rabbit psoas muscle. *Biophys. J.* 73: 2304–2312. https://doi.org/10.1016/S0006-3495(97)78262-6

Naber, N., R. Cooke, and E. Pate. 2011. Slow myosin ATP turnover in the super-relaxed state in tarantula muscle. *J. Mol. Biol.* 411:943–950. https://doi.org/10.1016/j.jmb.2011.06.051

Padrón, R., W. Ma, S. Duno-Miranda, N. Koubassova, K.H. Lee, A. Pinto, L. Alamo, P. Bolaños, A. Tsaturyan, T. Irving, and R. Craig. 2020. The myosin interacting-heads motif present in live tarantula muscle explains tetanic and posttetanic phosphorylation mechanisms. *Proc. Natl. Acad. Sci. USA.* 117:11865–11874. https://doi.org/10.1073/pnas.1921312117

Pettersen, E.F., T.D. Goddard, C.C. Huang, G.S. Couch, D.M. Greenblatt, E.C. Meng, and T.E. Ferrin. 2004. UCSF Chimera--a visualization system for exploratory research and analysis. *J. Comput. Chem.* 25:1605–1612. https://doi.org/10.1002/jcc.20084

Ratkowsky, D.A., J. Olley, and T. Ross. 2005. Unifying temperature effects on the growth rate of bacteria and the stability of globular proteins. *J. Theor. Biol.* 233:351–362. https://doi.org/10.1016/j.jtbi.2004.10.016

Robert-Paganin, J., O. Pylypenko, C. Kikuti, H.L. Sweeney, and A. Houdusse. 2020. Force generation by myosin motors: a structural perspective. *Chem. Rev.* 120:5–35. https://doi.org/10.1021/acs.chemrev.9b00264

Ruhland, M.R.R. 1978. Die Beinmuskulatur und ihre Innervation bei der VogelspinneDugesiella hentzi (Ch.) (Araneae, Avicula riidae). *Zoomorphologie.* 89:33–46. https://doi.org/10.1007/BF00993780

Schartau, W., and T. Leidescher. 1983. Composition of the hemolymph of the tarantula *Eurypelma californicum*. *J. Comp. Physiol.* 152:73–77. https://doi.org/10.1007/BF00689730

Shimomura, T., H. Iwamoto, T.T. Vo Doan, S. Ishiwata, H. Sato, and M. Suzuki. 2016. A beetle flight muscle displays leg muscle microstructure. *Biophys. J.* 111:1295–1303. https://doi.org/10.1016/j.bpj.2016.08.013

Stewart, M.A., K. Franks-Skiba, S. Chen, and R. Cooke. 2010. Myosin ATP turnover rate is a mechanism involved in thermogenesis in resting skeletal muscle fibers. *Proc. Natl. Acad. Sci. USA.* 107:430–435. https://doi.org/10.1073/pnas.0909468107

Sulbarán, G., A. Biasutto, L. Alamo, C. Riggs, A. Pinto, F. Méndez, R. Craig, and R. Padrón. 2013. Different head environments in tarantula thick filaments support a cooperative activation process. *Biophys. J.* 105: 2114–2122. https://doi.org/10.1016/j.bpj.2013.09.001

Sulbarán, G., A. Biasutto, F. Méndez, A. Pinto, L. Alamo, and R. Padrón. 2020. $^{18}O$ labeling on Ser45 but not on Ser35 supports the cooperative phosphorylation mechanism on tarantula thick filament activation. *Biochem. Biophys. Res. Commun.* 524:198–204. https://doi.org/10.1016/j.bbrc.2020.01.044

Tanaka, H., T. Kobayashi, Y. Amemiya, and K. Wakabayashi. 1986. Time-resolved X-ray diffraction studies of frog skeletal muscle isometrically twitched by two successive stimuli using synchrotron radiation. *Biophys. Chem.* 25:161–168. https://doi.org/10.1016/0301-4622(86)87006-5

van Dijk, E., A. Hoogeveen, and S. Abeln. 2015. The hydrophobic temperature dependence of amino acids directly calculated from protein structures. *PLOS Comput. Biol.* 11:e1004277. https://doi.org/10.1371/journal.pcbi.1004277

Wendt, T., D. Taylor, K.M. Trybus, and K. Taylor. 2001. Three-dimensional image reconstruction of dephosphorylated smooth muscle heavy meromyosin reveals asymmetry in the interaction between myosin heads and placement of subfragment 2. *Proc. Natl. Acad. Sci. USA.* 98:4361–4366. https://doi.org/10.1073/pnas.071051098

Woodhead, J.L., F.Q. Zhao, R. Craig, E.H. Egelman, L. Alamo, and R. Padrón. 2005. Atomic model of a myosin filament in the relaxed state. *Nature.* 436:1195–1199. https://doi.org/10.1038/nature03920

Wray, J.S., P.J. Vibert, and C. Cohen. 1975. Diversity of cross-bridge configurations in invertebrate muscles. *Nature.* 257:561–564. https://doi.org/10.1038/257561a0

Xu, S., J. Gu, T. Rhodes, B. Belknap, G. Rosenbaum, G. Offer, H. White, and L.C. Yu. 1999. The M.ADP.Pi state is required for helical order in the thick filaments of skeletal muscle. *Biophys. J.* 77:2665–2676. https://doi.org/10.1016/S0006-3495(99)77101-8

Xu, S., G. Offer, J. Gu, H.D. White, and L.C. Yu. 2003. Temperature and ligand dependence of conformation and helical order in myosin filaments. *Biochemistry.* 42:390–401. https://doi.org/10.1021/bi026085t

Zoghbi, M.E., J.L. Woodhead, R. Craig, and R. Padrón. 2004. Helical order in tarantula thick filaments requires the "closed" conformation of the myosin head. *J. Mol. Biol.* 342:1223–1236. https://doi.org/10.1016/j.jmb.2004.07.037

# Supplemental material

Video 1. **Dissection details of the flexor femoris cbensis muscle of *A. hentzi*.** The video is played back in real time.